

# Abstracts



11th National Norwegian NMR Meeting  
Golsfjellet, Norway, 18-20 January 2010

## Program NMR2010

### Monday

09.00-13.00 **Registration**  
13.00-14.00 **Lunch**  
14.00-14.15 **Welcome**

#### Session 1: **Biomolecular liquid NMR**

**Chairman: Nils Åge Frøystein/Lars Skjeldal**

14.15-14.35 **Aurora Martinez** The solution structure of the regulatory subunit of PKA  
14.35-14.55 **Lars Skjeldal** NMR studies of metal binding to kalata B1.  
14.55-15.15 **Alexander Dikiy** Functional Insights into the Catalytic Mechanism of Methionine Sulfoxide Reductase B1 through its Structural Analysis  
15.15-15.35 **Jarl Underhaug** Structural characterization of a vision-impairing protein using liquid-state NMR  
15.35-16.05 **Coffee break**  
16.05-16.25 **Annette Brenner** Multi-nuclear and multi-dimensional NMR-spectroscopy studies of two medium-sized proteins  
16.25-16.45 **Per E. Kristiansen** Structure Function of two Peptide Bacteriocins  
16.45-17.05 **Nebojsa Simic**  $^1\text{H}$ ,  $^{13}\text{C}$  and  $^{19}\text{F}$  NMR data of *N*-substituted 6-(4-methoxyphenyl)-7*H*-pyrrolo[2,3-*d*]pyrimidin-4-amines in DMSO-*d*<sub>6</sub>  
17.05-17.25 **Einar Sletten** Cisplatin Adducts on a GGG Sequence within a DNA Duplex  
17.25-17.45 **Øyvind Halskau** Dynamic, yet functional N-terminal domain of Tyrosine Hydroxylase examined by NMR  
17.45-19.30- **Poster session**  
**Dinner**

### Tuesday

09.00-13.00 **Skiing**  
13.00-14.00 **Lunch**

#### Session 2: **Medical NMR**

**Chairman: Ingrid S. Gribbestad**

14.00-14.20 **Torgils Fossen** The molecular weapons of influenza virus  
14.20-14.40 **Beathe Sitter** MR spectroscopy of breast cancer patients for prediction of treatment response – combining *in vivo* and *ex vivo* analysis  
14.40-15.00 **Martin Ystad** Age related changes in subcortical brain connectivity - a combined fMRI and DTI study  
15.00-15.20 **Hjørdis Skår** NMR examinations of potentially new contrast agents  
15.20-15.40 **Maria Grinde**  $^{13}\text{C}$  HR MAS MRS reveals differences in the glucose metabolism between two breast cancer xenograft models with different gene expression patterns  
15.40-16.00 **Lisa Drange-Hole** 7T MRI of the *ex vivo* perfused rat heart  
16.00-16.30 **Coffee break**  
16.30-17.40 **Special Session: Superhøyfelt NMR i Norge:** Introduction by Øyvind Halskau, UiB  
17.40-18.00 **Break**  
18.00-19.00 **Meeting in Norwegian Society of Magnetic Resonance**  
19.30- **Dinner**

### Wednesday

#### Session 3: **NMR of heterogeneous systems**

**Chairman: John G. Seland**

10.00-10.20 **Dick Sandström** Strategies to Increase the Sensitivity in NMR Spectroscopy  
10.20-10.40 **Signe Steinkopf** Amphiphilic drug interaction with glycerophospholipid studied by Solid-State NMR and the Langmuir monolayer technique  
10.40-11.00 **Eddy W. Hansen** Chain Diffusion in Semi-Crystalline Polymers  
11.00-11.30 **Coffee break**  
11.30-11.50 **Ketil Djurhuus** Dynamic NMR: Pore structure characterization and pore scale connectivity  
11.50-12.10 **Christian Totland** Water and Heptanol Interaction with a Non-porous Silica Surface: A  $^1\text{H}$  Solid State NMR Study  
12.10-12.30 **Willy Nerdal** Cisplatin interaction with phosphatidylserine bilayer studied by solid-state NMR spectroscopy  
12.30-14.00 **Lunch**

Monday

## **The solution structure of the regulatory subunit of PKA binding**

**In-Ja L. Byeon<sup>1</sup>, Khanh K. Dao<sup>2</sup>, Jinwon Jung<sup>1</sup>, Jeffrey Keen<sup>2</sup>, Ingar Leiros<sup>3</sup>, Stein O. Døskeland<sup>2</sup>, Aurora Martinez<sup>2</sup>, Angela M. Gronenborn<sup>1</sup>**

<sup>1</sup>Department of Structural Biology, University of Pittsburgh School of Medicine, Pittsburgh, PA 15260, USA; <sup>2</sup>Department of Biomedicine, University of Bergen, Jonas Lies vei 91, 5009-Bergen; <sup>3</sup>Norwegian Structural Biology Centre (Norstruct), Department of Chemistry, University of Tromsø, N-9037 Tromsø

The activation of protein kinase A involves the synergistic binding of cAMP to two cAMP binding sites on the inhibitory R subunit, causing release of the C subunit, which subsequently can carry out catalysis. We used NMR to structurally characterize the free and cAMP-bound RI $\alpha$ (98-381) subunit in solution and map the effects of cAMP binding at single residue resolution. Several conformationally disordered regions in free RI $\alpha$  become structured upon cAMP binding, including the  $\alpha$ C:A helix that connects domains A and B. NMR titration experiments with the B-site selective 2-Cl-8-hexylamino-cAMP, the A-site selective N<sup>6</sup>-monobutyryl-cAMP, and cAMP itself revealed structural consequences of binding to each site. Binding of ligand to the B- and A-sites induced  $\alpha$ C:A helix formation. In addition, A-site binding also affected residues within the B domain, suggesting several possible pathways of allosteric communication between the sites. The structural basis for the inter-domain communication is provided by amino acids whose side chains are lining the A domain binding site, such as Trp262, although their positions in the sequence place them in the B domain. Structuring of the  $\alpha$ C:A helix by nucleotide binding to either site reflects the synergistic interplay between the two sites, and may underlie the positive cooperativity of cAMP activation of the kinase.

# NMR STUDIES OF METAL BINDING TO KALATA B1.

**Lars Skjeldal**

*The Norwegian University of Life Sciences, UMB, Norway*

The use of the plant *Oldenlandia affinis* DC during childbirth was observed in the Lulua population of Kasai, Congo (Zaire) in 1960. The macrocyclic peptide Kalata B1 from *Oldenlandia affinis* DC, was discovered due to an active ingredient in a herbal medicine used by African women to assist childbirth.

The main peptide, Kalata B1, was isolated and characterized as a cyclic polypeptide, and comprised of 29 amino acid residues. The sequence was elucidated and three internal disulfide bridges were found which could explain the resistance against enzymatic degradation. 2D Nuclear Magnetic Resonance (NMR) studies revealed a three-dimensional structure composed of mainly beta-strands connected by tight turns. The polypeptide showed a characteristic biological activity on smooth muscle and on cardiac muscle, as well as a clear hemolytic activity. Here we show the binding of transition metals to Kalata B1.

Cyclic Peptides from *Oldenlandia affinis* DC. Molecular and Biological Properties

Gran L, Sletten K, Skjeldal L

(2008) CHEMISTRY & BIODIVERSITY Volume: 5 Issue: 10 Pages: 2014-2022

# Functional Insights into the Catalytic Mechanism of Methionine Sulfoxide Reductase B1 through its Structural Analysis

Finn L. Aachmann<sup>a</sup>, Lena S. Sal<sup>a</sup>, Hwa-Young Kim<sup>b</sup>, Vadim N. Gladyshev<sup>c</sup> and Alexander Dikiy<sup>a,\*</sup>

<sup>a</sup> Department of Biotechnology, Norwegian University of Science and Technology, N-7491 Trondheim, Norway, <sup>b</sup>Department of Biochemistry and Molecular Biology, Yeungnam University College of Medicine, Daegu 705-717, South Korea, and, <sup>c</sup> Department of Biochemistry, University of Nebraska, Lincoln, Nebraska 68588, USA.

Reactive oxygen species (ROS) can oxidize Met in proteins to a mixture of the *R*- and *S*-isomer of Met-sulfoxide (Met-SO). The Met-SO reductases (Msr) regenerate Met-SO back to Met in the presence of thioredoxin reductase (Trx). There are two different classes of Met-SO reductases: MsrA catalyses the reduction of the *S*-isomer while MsrBs reduce the *R*-form of Met-SO.

Mammalian MsrB1 contains Sec in the active site while MsrB2/3 are cysteine homologs of MsrB1, having a Cys instead of Sec in their active site. It was proposed that Sec and Cys forms of MsrBs proteins use different mechanisms to catalyze Met-SO reduction. The main objective of this project is to distinguish different catalytic mechanisms of mammalian MsrBs proteins.

Standard NMR experiments were used to obtain the resonance assignment on uniformly <sup>13</sup>C/<sup>15</sup>N labeled reduced recombinant Sec95Cys MsrB1. The structure calculations were based on geometrical constraints derived from NOE and angles constraints obtained from TALOS. The MsrB1<sub>red</sub> structure is characterized as an overall  $\beta$ -fold protein consisting of eight antiparallel  $\beta$ -strands. The first 18 amino acids in the N-terminal form a highly mobile tail.

The reaction mechanism for MsrB1 was studied by exposing it to both Met-SO (substrate) and Met-SO<sub>2</sub> (inhibitor). The observed results indicate that the Cys4 at the protein N-terminal tail acts as the resolving Cys reacting with the oxidized catalytic Sec. The protein's activity is then restored by reduction of the formed intramolecular seleno-sulpho bond by Trx.

The pH dependence of the active site residues was investigated in order to establish whether the same level of structural perturbation is present in MsrB1 compared to other MsrBs. It was found that Cys95 has around 2 pH unit lower pK<sub>a</sub> than a normal Cys. The accomplished studies together with the analysis of the data available for Cys-homologs of MsrB support the previously proposed suggestion that Sec-containing MsrB1 has different mechanism for MetSO reduction in comparison with Cys-containing MsrBs.

# Structural characterization of a vision-impairing protein using liquid-state NMR

Jarl Underhaug<sup>a,b</sup>, Kasper Runager<sup>c</sup>, Rajiv Vaid Basaiawmoit<sup>c</sup>, Torsten Kristensen<sup>c</sup>, Daniel Otzen<sup>c</sup>, Jan J. Enghild<sup>c</sup>, Anders Malmendal<sup>b</sup>, Niels Chr. Nielsen<sup>b,c</sup>

<sup>a</sup>Current Address: Department of Biomedicine, University of Bergen, Norway

<sup>b</sup>Department of Chemistry, inSPIN, and iNANO, University of Aarhus, Denmark

<sup>c</sup>Department of Molecular Biology, inSPIN, and iNANO, University of Aarhus, Denmark

---

## Abstract

FAS4 is the fourth fasciclin domain of transforming growth factor beta induced protein, a protein which is found in the extracellular matrix of most tissues. Several different mutations in the protein causes aggregations in the cornea, with the consequence of reduction or loss of eyesight. The aim of the project is to map the structural changes caused by mutations in FAS4, and thus achieve a better understanding of the mechanism behind the formation of the aggregates. A first step we have determined the three dimensional structure of the wild-type protein and the R555W mutant of this 14 kDa domain using liquid-state NMR. The two proteins have remarkably similar structures, but very different stability.

*Key words:* TGFBIp, FAS4, liquid-state NMR, Corneal dystrophy, Mutation

---

# **Multi-nuclear and multi-dimensional NMR-spectroscopy studies of two medium-sized proteins**

**Preliminary assignment results obtained from high-field NMR-spectroscopy and amino acid edited  $^1\text{H}$ - $^{15}\text{N}$  HSQC**

Annette Brenner<sup>1</sup>, Johan Lillehaug<sup>2</sup>, Arnt Johan Raae<sup>2</sup>, Rune Henrik Evjenth<sup>2</sup> and Nils Åge Frøystein<sup>1</sup>

<sup>1</sup>*Department of Chemistry, University of Bergen, Allégaten 41, N-5007 Bergen*

<sup>2</sup>*Department of Molecular Biology, University of Bergen, Thormøhlensgate 55, N-5008 Bergen*

Two doubly labelled ( $^{15}\text{N}$ ,  $^{13}\text{C}$ ) proteins are at the moment investigated at the University of Bergen: A 14 kDa spectrin and a 19 kDa acetyl transferase. The major goal of the project is to define the native structures of these proteins and to get insight into their functions by binding studies. About 80% of the backbone and the aliphatic sidechains of both proteins have been assigned so far.

In case of the spectrin, it was possible to achieve the backbone assignment exclusively by performing a standard set of 3D experiments – HNCA, HN(CO)CA, HNCOC, HN(CA)CO, HNCACB and CBCA(CO)NH – using a Bruker 600 MHz spectrometer equipped with cryoprobe at the University of Bergen.

Due to its size, the acetyl transferase showed less well-resolved peaks and more overlap in the third dimension than the spectrin. The  $^1\text{H}$ - $^{15}\text{N}$  HSQC assignment was accomplished by a series of MUSIC-experiments (Multiplicity Selective In-phase Coherence) and use of high-field spectroscopy in addition to the standard set of 3D experiments. MUSIC gains amino acid specific  $^1\text{H}$ - $^{15}\text{N}$  HSQC spectra, i.e. spectra that only contain peaks belonging to one amino acid or to a group of amino acids that show spin system similarities, whilst suppressing all the other signals. In addition, the standard set of 3D experiments was also performed using a Varian 800 MHz spectrometer at the Swedish NMR centre, University of Gothenburg. This resulted in an improvement of the resolution in the third dimension and made it possible to assign peaks in the regions with high signal overlap.

## Structure Function of two Peptide Bacteriocins

Per Eugen Kristiansen, Per Rogne, Nina Fimland, Camilla Oppegård, Christofer Haugen and Jon Nissen-Meyer, Department of Molecular Biosciences University of Oslo, Norway

Bacteria-produced anti-microbial peptides (AMPs), generally referred to as bacteriocins, are able to kill bacteria at pico- to nano-molar concentrations, and have thus been suggested as alternatives to commonly used antibiotics. Bacteriocins produced by lactic acid bacteria (LAB) have drawn special attention. These LABs are present in the human diet and are a part of the intestinal microbial flora, and are thus generally regarded as safe for humans. The LAB produces several antimicrobial peptides. Two bacteriocins produced by LAB, nisin and pediocin PA-1, have been approved as food additives in the European Union and the US.

The LAB bacteriocins are generally cationic, 25 to 60 amino acid residues long, and kill bacteria by permeabilizing the cell membrane. The two-peptide bacteriocins are unique in that they, as the name suggests, require the presence of two different peptides in approximately equal amounts to exert optimal antimicrobial activity. The peptides on their own have no, or very low, activity and appear to act by forming an active complex.

Bacteriocins are unstructured in water but become structured in membrane mimicking environments. In our lab we have determined the structures of the two peptide bacteriocins Plantaricin EF, Plantaricin JK and Lactococcin G in TFE and DPC by NMR. Each bacteriocin consists of two structurally different peptides. All the six peptides have partly helical structures as determined by NMR. Based on the peptide structures possible bacteriocin structures have been proposed.

All two peptide bacteriocins now contain one or more GxxxG motif. This motif is known as a helix-helix interaction motif in transmembrane proteins. We have done mutational analysis to these motifs in Plantaricin JK and Lactococcin G to determine to what extent they are important to the antimicrobial activity of the bacteriocins. The result from the structural and mutational studies will be discussed.

# $^1\text{H}$ , $^{13}\text{C}$ and $^{19}\text{F}$ NMR data of *N*-substituted 6-(4-methoxyphenyl)-7*H*-pyrrolo[2,3-*d*]pyrimidin-4-amines in $\text{DMSO-}d_6$

Christopher Sørum,<sup>a,b</sup> Nebojša Simić,<sup>a</sup> Eirik Sundby,<sup>c</sup> and Bård Helge Hoff<sup>a</sup>

a) Norwegian University of Science and Technology, Høgskoleringen 5, NO-7491 Trondheim, Norway

b,c) Current adress: Weifa AS, Guveveien 1, 3791 Kragerø, Norway.

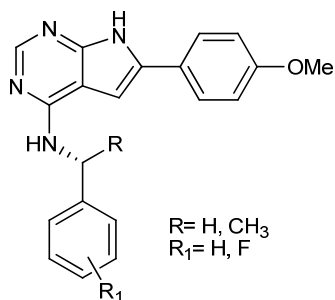
c) Sør-Trøndelag University College, E. C. Dahls gate 2, 7004 Trondheim, Norway.

**Keywords:** NMR;  $^1\text{H}$ ;  $^{13}\text{C}$ ;  $^{19}\text{F}$ ; 7*H*-pyrrolo[2,3-*d*]pyrimidin-4-amines.

## Abstract

Tyrosine kinases (TK) are enzymes which bind ATP and catalyse the transfer of  $\gamma$ -phosphate to hydroxy groups of tyrosine residues in proteins, regulating their activity and function. Several tyrosine kinases can be targets for cancer chemotherapy, the most important being the receptor tyrosine kinases (RTK).<sup>1</sup> This is a large family of receptors including, among others, the epidermal growth factor receptor (EGFR),<sup>2,3</sup> and the vascular endothelial growth factor receptor.<sup>4</sup> Pyrrolopyrimidines have shown promising properties as tyrosine kinase inhibitors.<sup>5-8</sup>

Further, there is evidence that such compounds or analogues have prospects of becoming efficient antiprotozoal agents.<sup>9</sup> Another interesting finding is the that the ErbB2 tyrosine kinase is involved in developing leprosy, and that the breakdown of myelin causing the disease can be blocked by kinase inhibitors.<sup>10, 11</sup> On this background we have undertaken the synthesis and characterisation of seven pyrrolopyrimidines, and present herein their NMR spectroscopic properties.



1. D. Mukherji, J. Spicer, *Expert Opin. Invest. Drugs* **2009**, 18, 293.
2. P. S. Sharma, R. Sharma, T. Tyagi, *Curr. Pharm. Des.* **2009**, 15, 758.
3. R. Bose, X. Zhang, *Exp. Cell Res.* **2009**, 315, 649.
4. V. L. Keedy, A. B. Sandler, *Cancer Sci.* **2007**, 98, 1825.
5. Caravatti, G. New 7*H*-Pyrrolo[2,3-*d*]Pyrimidines Inhibiting ErbB and VEGF Receptor Tyrosine Kinases. **2004**, Abstracts, 36th Central Regional Meeting of the American Chemical Society, Indianapolis, IN, United States.
6. M. Croyle, N. Akeno, J. A. Knauf, D. Fabbro, X. Chen, J. E. Baumgartner, H. A. Lane, J. A. Fagin, *Cancer Res.* **2008**, 68, 4183.
7. P. Traxler, P. R. Allegrini, R. Brandt, J. Brueggen, R. Cozens, D. Fabbro, K. Grosios, H. A. Lane, P. McSheehy, J. Mestan, T. Meyer, C. Tang, M. Wartmann, J. Wood, G. Caravatti, *Cancer Res.* **2004**, 64, 4931.
8. X. Cai, C. Qian, S. Gould, WO 2008033745, **2007**.
9. K. Mensa-Wilmot, WO 2008066755, **2007**.
10. N. Tapinos, M. Ohnishi, A. Rambukkana, *Nature Med.* **2006**, 12, 961.
11. J. M. Franklin Robin, C. Zhao, *Nature Med.* **2006**, 12, 889.

## Cisplatin Adducts on a GGG Sequence within a DNA Duplex.

Tormod Skauge<sup>1</sup>, Einar Sletten<sup>1</sup>, Stephane Teletcha<sup>2</sup>, and Jiri Kozelka<sup>2</sup>

<sup>1</sup>Department of Chemistry, University of Bergen

<sup>2</sup>Laboratoire de Chimie et Biochimie, Université Paris Descartes.

**Abstract:** The antitumor drug cisplatin (cis-[PtCl<sub>2</sub>(NH<sub>3</sub>)<sub>2</sub>]) reacts with cellular DNA to form GG intrastrand adducts between adjacent guanines as predominant lesions. GGG sites have been shown to be hotspots of platination [1-2]. To study the structural perturbation induced by binding of cisplatin to two adjacent guanines of a GGG trinucleotide, we have examined the duplex [(G<sub>1</sub>C<sub>2</sub>C<sub>3</sub>G\*<sub>4</sub> G\*<sub>5</sub> G<sub>6</sub>T<sub>7</sub>C<sub>8</sub>G<sub>9</sub>C<sub>10</sub>) · d(G<sub>11</sub>C<sub>12</sub>G<sub>13</sub>A<sub>14</sub>C<sub>15</sub>C<sub>16</sub>C<sub>17</sub>G<sub>18</sub>G<sub>19</sub>C<sub>20</sub>)] (dsCG\*G\*G) intrastrand cross-linked at the G\* guanines by cis-{Pt(NH<sub>3</sub>)<sub>2</sub>}<sup>2+</sup> using NMR spectroscopy and molecular dynamics (MD) simulations. The NMR spectra of dsCG\*G\*G were found to be similar to those of previously characterized DNA duplexes cross-linked by cisplatin at a pyG\*G\*X site (py=pyrimidine; X=C,T, A). This similarity of NMR spectra indicates that the base at the 3'-side of the G\*G\*-Pt cross-link does not affect the structure to a large extent. An unprecedented reversible isomerisation between the duplex dsCG<sub>4</sub>\*G<sub>5</sub>\*G and duplex dsGG<sub>5</sub>\*G<sub>6</sub>\*T was observed, which yielded a 40:60 equilibrium between the two intrastrand GG-Pt cross-links. No formation of interstrand cross-links was observed. The NMR spectroscopic chemical shifts of dsGG\*G\*T showed some fundamental differences to those of pyG\*G\*-platinum adducts but were in agreement with the NMR spectra reported previously for the DNA duplexes crosslinked at an AG\*G\*C sequence by cisplatin or oxaliplatin. significantly.

[1] S. O. Ano, Z. Kuklenyik, L. G. Marzilli. In: Cisplatin: Chemistry and Biochemistry of a Leading Anticancer Drug (Ed.: B. Lippert), Verlag Helvetica Chimica Acta, Zurich, 1999, pp. 247 –291.

[2] M.-A. Elizondo-Riojas, J. Kozelka, *J. Mol. Biol.* 2001, 314, 1227 –1243.

Dynamic, yet functional N-terminal domain of Tyrosine Hydroxylase examined by NMR

Øyvind Halskau<sup>1</sup>, Jarl Underhaug<sup>1</sup>, Knut Teigen<sup>1</sup>, Lars Skjærven<sup>1</sup>, and Aurora Martínez<sup>1</sup>

<sup>1</sup> Department of Biomedicine, Faculty of Medicine, University of Bergen

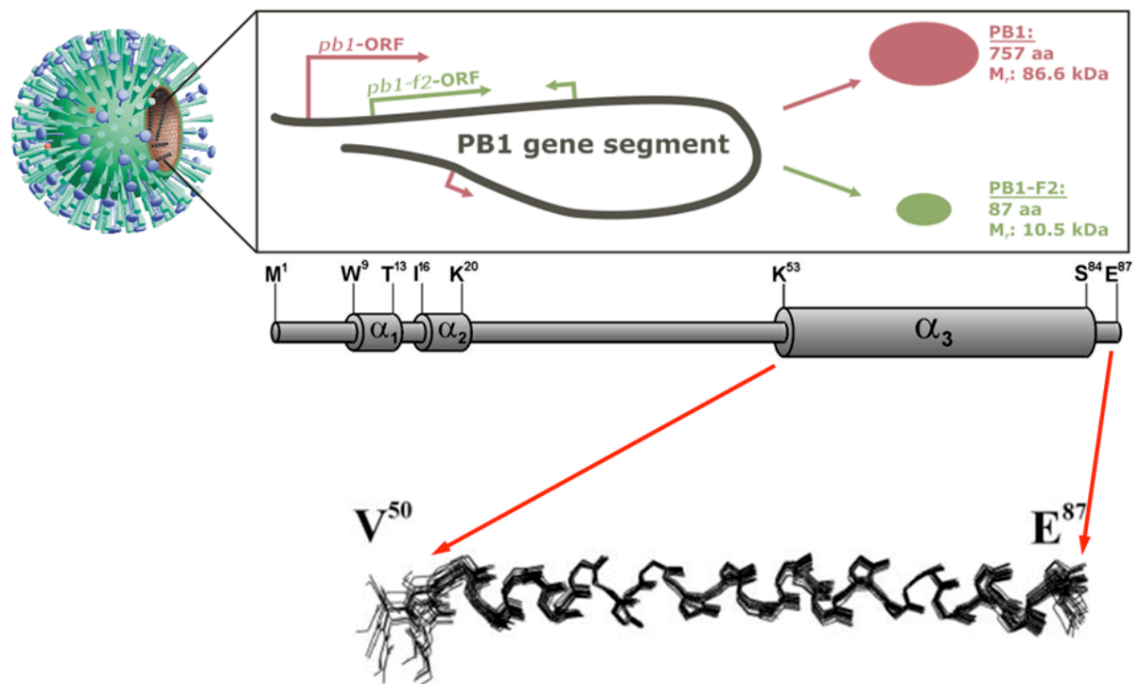
Tyrosine Hydroxylase (TH) is the rate-determining enzyme in the synthesis of catecholamines, and hence very important in the function of sympathetic nervous system. It is normally a soluble, tetrameric protein dependent of O<sub>2</sub>, Fe<sup>2+</sup> and tetrahydrobiopterine for its function. We have recently established that 14-3-3gamma – one isoform out of seven human variants – mediates a controlled localization of TH to the membrane. The 14-3-3s are a class of proteins that have important scaffolding roles in cell signalling, and thus influence function in ways that are being intensively investigated. TH interacts with 14-3-3 through its N-terminal domain consisting of 43 amino acids, provided that Serine 19 is phosphorylated. Without the phosphorylation, and in the absence of 14-3-3, TH still locates to the membrane, but without 14-3-3gamma it causes a rapid and complete membrane disruption that probably is very damaging should this occur in an organisms synaptic membrane. There are clear links between this phenomenon and several neurodegenerative diseases, including Parkinson's. The part of TH that simultaneously mediates binding to 14-3-3gamma and the membrane is a domain that up to now has been a structural unknown. We initiated the NMR study to gain insight into the structure and dynamics of the phosphorylated and unphosphorylated peptide. The two peptide forms, while relatively unstructured, are clearly distinct from each other. We attempt a rationalization of both its 14-3-3 binding and membrane binding behaviour based on the structures solved using NOESY restraints from unlabelled and partially <sup>15</sup>N-labelled samples as restraints input into AMBER simulations.

Tuesday

# The molecular weapons of influenza virus

Torgils Fossen, Karsten Bruns, Nicole Studtrucker, Alok Sharma, Rene Röder, Sara Marie Øie Solbak, David Mitzner, Friedrich Hahn, André Eissmann, Uwe Tessmer, Peter Henklein, Victor Wray, Ulrich Schubert

The influenza A virus (IAV) triggers global flu epidemics again and again, killing tens of thousands, sometimes millions of people. Researchers at Helmholtz Center for Infection Research in Braunschweig, the University of Erlangen-Nürnberg, Heinrich-Pette-Institute, Hamburg, Institute of Biochemistry, Charité Universitätsmedizin-Berlin and the Pharmacognosy research group at Centre for pharmacy, Department of Chemistry, University of Bergen have now thoroughly investigated one of the molecular 'weapons', which targets the pathogen for us. Our analysis of the IAV-molecule PB1-F2 revealed that this protein may at least be partly responsible for the devastating effects of the virus. PB1-F2 appears to cause harm to the host cell membranes and can therewith cause the death of the cell. This may be particularly important since other disease-causing viruses have proteins with very similar function. Under certain circumstances the harmful effects of various viral infections may therefore be based on very similar molecular basis.



Schematic depiction of influenza A virus (IAV) and expression of PB1-F2 by the use of an alternative (+1) open reading frame (ORF) on the RNA polymerase basic protein 1 (PB1) gene segment. Structure of PB1-F2 shown was determined by NMR spectroscopy.

## References

K. Bruns, N. Studtrucker, A. Sharma, T. Fossen, D. Mitzner, A. Eissmann, U. Tessmer, R. Roder, P. Henklein, V. Wray, U. Schubert: Structural characterization and Oligomerization of PB1-F2, a pro - apoptotic influenza A virus protein. *Journal of Biological Chemistry*, 2007, 282, 353-363.

R. Röder, K. Bruns, A. Sharma, A. Eissmann, F. Hahn, N. Studtrucker, T. Fossen, V. Wray, P. Henklein, U. Schubert (2008). Synthesis of full length PB1-F2 influenza A virus proteins from 'Spanish flu' and 'bird flu'. *Journal of Peptide Science* 14, 954-962.

# MR spectroscopy of breast cancer patients for prediction of treatment response – combining *in vivo* and *ex vivo* analysis

B. Sitter<sup>1</sup>, M. G. Heldahl<sup>1</sup>, T. F. Bathen<sup>1</sup>, A. Bofin<sup>2</sup>, S. Lundgren<sup>1,3</sup>, and I. S. Gribbestad<sup>1</sup>

<sup>1</sup>Department of Circulation and Medical Imaging, Norwegian University of Science and Technology, Trondheim, Norway, <sup>2</sup>Department of Laboratory Medicine, Children's and Women's Health, Norwegian University of Science and Technology, Trondheim, Norway, <sup>3</sup>Department of Oncology, St. Olavs University Hospital

## Background

The overall prognosis for breast cancer is good, but 45 % of patients with locally advanced breast cancer die within five years (1). Breast cancer care would improve by better stratification of patients to different therapies and more efficient evaluation of treatment effects. Tissue concentrations of total choline (tCho) in breast cancers have the potential to predict treatment response and be a measure of treatment effects (2). We wanted to combine *in vivo* and *ex vivo* MR spectroscopy (MRS) of breast cancer patients assigned for neoadjuvant chemotherapy (NAC) to investigate the correlation between tCho levels detected *in vivo* and *ex vivo*.

## Experimental

Patients (n=35) with locally advanced breast cancer (stage T3 or T4) assigned for NAC (FEC: 5-Fluorouracil, Epirubicine and Cyclophosphate) were included in the study. Tumor size was measured clinically the day prior to treatment and after the last chemotherapeutic dose. The Regional Committee for Medical and Health Research Ethics approved the study protocol, and all patients provided written informed consent. *In vivo* <sup>1</sup>H MRS was performed before NAC at a 3T Siemens Trio system (Siemens, Germany). The spectra were obtained using the standard PRESS sequence (TE=135, TR=2000 ms and NS=128). Core needle biopsies were taken prior to the first treatment from the same patients. Tissue samples were placed in cryogenic vials and immersed in liquid nitrogen immediately after dissection. *Ex vivo* HR MAS MRS was performed on tissue samples as previously described (3). Peak areas were determined using curve fitting (PeakFit, Seasolve; USA), and concentrations of glycerophosphocholine (GPC), phosphocholine (PCho) and choline were determined using ERETIC (3). Tissue imprints were made on glass slides before sample preparation and HR MAS analysis. The imprints were evaluated by a pathologist after staining with a modified May-Grünwald-Giemsa stain (Color Rapid, Med-Kjemi; Norway) and scored as malignant, suspicious of malignancy, DCIS, non-malignant or of insufficient quality for evaluation. Only patients with biopsies scored as malignant, suspicious of malignancy or DCIS were included in the study, resulting in *in vivo* and *ex vivo* MRS data from 19 patients.

## Results

*In vivo* tCho was detected in 10 of 19 patients (SNR > 2). Tissue metabolites could be quantified using HR MAS in nine of these patients. *In vivo* MRS did not detect tCho in nine patients, where tissue metabolites could be quantified in seven of the HR MAS spectra. Comparing findings obtained *in vivo* and *ex vivo* showed that concentrations of tCho determined by *ex vivo* MRS were significantly higher in tissue from patients with detectable tCho levels *in vivo* (Table 1). Seven of the patients had complete clinical response. These patients had significant higher tissue concentration of GPC (p=0,037) than patients not having complete response (n=12), Figure 1. The higher tCho concentrations in clinical complete responders were not significantly different from those with less than complete response (p=0,066).

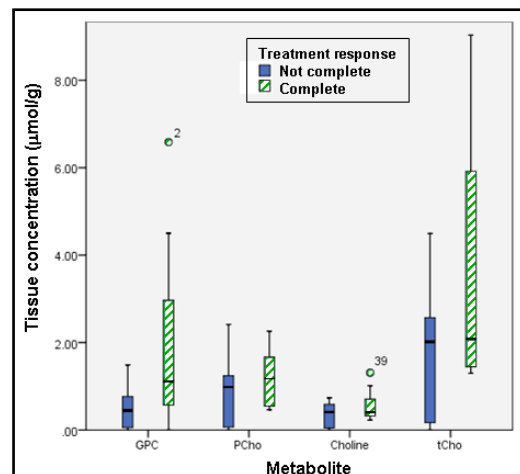


**Figure 1** Box-plot presentation of tissue metabolic concentrations in biopsies obtained before NAC for patients with different clinical response.

**Table 1** Tissue concentrations (µmol/g) of choline compounds in biopsies from patients with *in vivo* MRS detectable (SNR>2) and undetectable (SNR<2) levels of total choline.

	GPC	PCho	Choline	tCho
SNR > 2 (N= 10)	1,63 (±2,15)	1,31 (±0,81)	0,60 (±0,37)	3,55 (±2,90)
SNR < 2 (N=9)	0,48 (±0,54)	0,65 (±0,67)	0,24 (±0,18)	1,37 (±1,27)
p (Student's t-test)	0,138	0,068	0,019	0,054

## Discussion and Conclusion

*Ex vivo* and *in vivo* findings were consistent and demonstrate that *in vivo* MRS and *ex vivo* MRS of breast cancer describe the same features of a tumor. The finding of higher tissue concentrations of GPC in biopsies from patients with complete response to NAC is similar to previous findings in breast cancer biopsies (4). GPC might be a biomarker for treatment response in breast cancer patients receiving NAC.

## References

1 Giordano *The Oncologist* (2003) 8:421-530. 2 Haddadin et al. *NMR Biomed* (2009) 22: 65-76. 3 Sitter et al. *NMR Biomed* Accepted 2009. 4 Cao et al. [abstract]. *Proc Intl Soc Mag Reson Med* (2009), 17:417.

## **Age related changes in subcortical brain connectivity - a combined fMRI and DTI study**

Martin Ystad(1), Erlend Hodneland(1), Tom Eichele(2), Judit Haasz(1,2),  
Astri J. Lundervold(2), Arvid Lundervold(1,3)

1: Department of Biomedicine, Neuroinformatics and Image Analysis Laboratory

2: Department of Biological and Medical Psychology

University of Bergen, Jonas Lies vei 91, 5009 Bergen, Norway

3: Department of Radiology, Haukeland University Hospital, Bergen, Norway

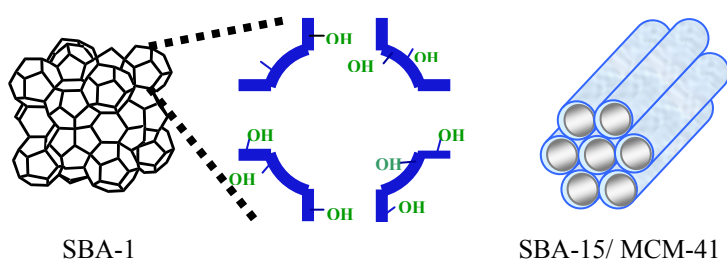
Normal aging leads to microscopic and macroscopic changes in all tissue types in the human brain. Qualitative changes in white matter have been assessed by diffusion tensor imaging (DTI), revealing reduced microstructural integrity as measured by decreased fractional anisotropy (FA) and increased mean diffusivity (MD). These changes are interpreted as reductions in the global structural connectivity in the brain. Recently, resting state fMRI has emerged as a method of investigating human brain functional connectivity. Spatially independent sources of activity, called resting state networks (RSNs), can be identified in the resting state using independent component analysis. It has been shown that the functional connectivity between RSNs decline in normal aging. In this study, we investigate age related connectivity changes in a cohort of 100 healthy elderly using a 1.5 T clinical scanner equipped with an eight-channel head coil. We particularly focus on the subcortical gray matter structures due to their extensive global connectivity. By combining measures from spatially co-registered DTI and resting state fMRI time courses with detailed anatomical segmentations, we report changes in both structural and functional connectivity within these structures.

## NMR examinations of potentially new contrast agents

Hjørdis Skår and John G. Seland

*Kjemisk Institutt, University of Bergen, Allegaten 41, N-5007 Bergen, Norway*

Nanosized periodic mesoporous silica (PMS) materials loaded with gadolinium have shown promising properties as potential contrast agents for magnetic resonance imaging, due to their ability to provide high contrast enhancement.<sup>1</sup> In this study, the gadolinium based porous hybrid materials are obtained by the controlled grafting of the metalorganic precursor  $\text{Gd}[\text{N}(\text{SiHMe}_2)_2]_3(\text{THF})_2$  onto the surface of PMS-materials SBA-1, SBA-15 and MCM-41.<sup>2</sup> The mesoporous support materials are characterised (via powder x-ray diffraction, nitrogen physisorption, transmission electron microscopy, scanning electron microscopy and FTIR spectroscopy) with different pore topologies, internal size distributions and particle sizes. The Gd content of the materials is kept low (1 %), giving high relaxivities compared to the commercial contrast agent Magnevist. A clear difference in relaxivity is observed with change of support materials, and our interest lies in the examination of the detailed relaxation mechanisms of differently structured PMS materials. The key to a better understanding of the underlying mechanisms in these potentially new contrast agents is to use NMR to investigate the local dynamical interaction between water and the metal ion. This is achieved by performing dynamic NMR experiments (diffusion and relaxation) and examining temperature and field dependence. The method of relaxography will also be used to investigate the equilibrium water exchange in phantoms and *in vivo*.<sup>3</sup>



**Scheme:** Porous, cubic structure of SBA-1 and porous, hexagonal structure of SBA-15/MCM-41

<sup>1</sup> a) Lin, Y. S.; Hung, Y.; Su, J. K.; Lee, R.; Chang, C.; Lin, M. L.; Mou, C. Y. *J.Phys.Chem. B* **2004**, *108*, 15608. b) Rieter, W. J.; Kim, J. S.; Taylor, K. M. L.; An, H.; Lin, W.; Tarrant, T. *Angew.Chem. Int. Ed.* **2007**, *46*, 3680. c) Carniato, F.; Tei, L.; Dastrù, W.; Marchese, L.; Botta, M. *Chem. Commun.* **2009**, *10*, 1246.

<sup>2</sup> (a) Kresge, C. T.; Leonowicz M. E.; Roth W. J.; Vartuli J. C.; Beck J. S.; *Nature*, **1992**, *359*, 710. (b) Zhao D.; Feng J.; Huo, Q.; Melosh, N.; Frederickson G.H.; Chmelka B.F.; Stucky G.D.; *Science*, **1998**, *279*, 548. (c) Huo Q.; Margolese D. I.; Ciesla U.; Feng P.; Gier T.E.; Sieger P.; Leon R.; Petroff P. M.; Schüth F.; Stucky G.D.; *Nature*, **1994**, *368*, 317.

<sup>3</sup> a) Seland, J. G.; Bruvold, M.; Brurok, H.; Jynge, P.; Krane J.; *Magn. Reson. in Medicine*, **2007**, *58*, 674. b) Pavlin T.; Bruvold, M.; Jynge, P.; Seland, J. G. *Proc. Intl. Soc. Mag. Reson. Med.* **2008**, *16*. c) Seland J. G.; Bruvold, M.; Skarra, S.; Brurok, H.; Jynge, P. *Proc. Intl. Soc. Mag. Reson. Med.* **2008**, *16*.

# <sup>13</sup>C HR MAS MRS reveals differences in the glucose metabolism between two breast cancer xenograft models with different gene expression patterns

Grinde MT<sup>1</sup>, Moestue SA<sup>1</sup>, Risa Ø<sup>1</sup>, Engebraaten O<sup>2</sup>, Gribbestad IS<sup>1</sup>

<sup>1</sup>Dept. of Circulation and Medical Imaging, NTNU, Trondheim, Norway

<sup>2</sup>Dept. of Tumor Biology, Cancer Research Institute, Oslo, Norway

## Introduction

Two breast cancer xenograft models have been established from human breast cancer patients and orthotopically xenografted in female SCID mice (1). The models represent a basal-like (poor prognosis) and a luminal-like (better prognosis) genetic profile. Using HR MAS <sup>1</sup>H MR spectroscopy, it has been shown that these two models have distinct metabolic profiles (2). It is well known that tumor cells metabolize glucose at a higher rate than normal cells (3). This is mainly used to form lactate and alanine and is observed even when high concentrations of oxygen are present. Labelled [<sup>13</sup>C]-glucose can be used to measure glucose consumption and transformation with MR spectroscopy. The purpose of this work was to investigate the rate of glucose metabolism in the two breast cancer xenograft models.

## Methods

Mice carrying xenograft tumors received a bolus injection of [1-<sup>13</sup>C]-glucose (29 mg per animal) via the lateral tail vein under isoflurane anaesthesia. 10 or 15 minutes after the injection, the mice were sacrificed and the tumor tissue harvested and immediately frozen in liquid nitrogen. A total of 33 samples were collected (N=19 controls from 19 animals, N=14 [1-<sup>13</sup>C]-glucose labelled from eight animals). One dimensional HR MAS <sup>1</sup>H with water presaturation and <sup>13</sup>C power gated proton decoupled MR spectra were recorded using a BRUKER Avance DRX600 with a <sup>1</sup>H/<sup>13</sup>C HR MAS probe. Two dimensional HSQC <sup>1</sup>H/<sup>13</sup>C coupled experiments were obtained on two samples for spectral assignment. All spectra were preprocessed, mean normalized, peak aligned and baseline corrected. Integration was performed to calculate metabolites ratios. A two sided t-test was performed to investigate differences in glucose, alanine and lactate between the groups.

## Results

A significant difference in the glucose/alanine ratio ( $p < 0.001$ ) between the luminal ( $0.43 \pm 0.33$ , N=9) and the basal-like ( $1.55 \pm 0.57$ , N=10) model was observed in the natural abundance spectra. It was a trend of higher glucose/lactate ratio in the basal-like ( $0.24 \pm 0.10$ ) compared to the luminal-like ( $0.13 \pm 0.18$ ) model, but no significant difference was observed. The difference in alanine/lactate was small between the two models. The [1-<sup>13</sup>C]-glucose labelled spectra had higher signals from glucose, alanine and lactate compared to the natural abundance spectra indicating an efficient glucose uptake and conversion. In the labelled spectra from samples collected after 15 minutes, differences between the two models (luminal-like N=6, basal-like model N=5) were observed. There was a trend of a higher glucose/alanine and glucose/lactate ratios between samples collected at 10 (N=3) and 15 (N=5) minutes in the basal-like model.

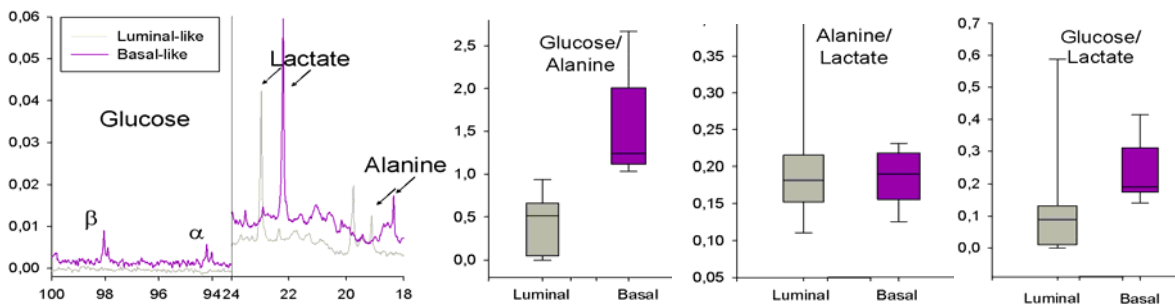


Figure 1: Average <sup>13</sup>C natural abundance spectra (expanded) and box plots of metabolite ratios from the luminal- and basal-like models indicate differences in glucose/alanine, glucose/lactate and alanine/lactate ratios between the two models.

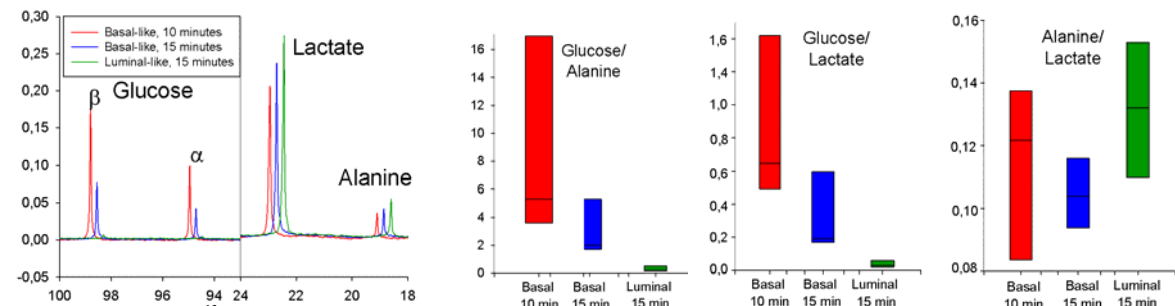


Figure 2: Average [1-<sup>13</sup>C]-glucose enriched spectra (expanded) and box plots of metabolite ratios from the two animal models showing the glucose/alanine, glucose/lactate and alanine/lactate ratios in samples from the two models harvested 10 or 15 minutes after injection of <sup>13</sup>C labelled glucose.

## Discussion

The natural abundance spectra indicate a higher glucose/alanine and glucose/lactate level in the basal-like compared to the luminal-like model. It is likely that a difference in the metabolite ratios between the two models is due to a lower concentration of glucose in the luminal-like model, glucose could in fact not be detected in several spectra. It was only a small difference in the alanine/lactate ratio between the two models.

There is a clear signal enhancement in glucose, lactate and alanine in the <sup>13</sup>C labelled spectra compared to the natural abundance spectra, indicating that glucose has been taken up and metabolised to lactate and alanine. No other <sup>13</sup>C labelled signals could be observed (data not shown). The difference in glucose/alanine and glucose/lactate ratios between the luminal-like and the basal-like model could be explained by a lower uptake of glucose and/or a higher rate of glucose metabolism towards lactate and alanine in the luminal-like compared to the basal-like model. The luminal-like model tends to convert almost all of the glucose to lactate and alanine within 15 minutes. In the basal-like model conversion from glucose to lactate and alanine is observed also between 10 and 15 minutes.

In conclusion, ex vivo <sup>13</sup>C MRS measurements demonstrate differences in the glucose metabolism for two different phenotypic breast cancer xenograft models.

## References

(1) Bergamashi et al. Mol Oncol 2009; 3:469-82 (2) Moestue et al. Proc Int Soc Magn Reson Med, Honolulu 2009, #2323 (3) Warburg Science 1956; 123: 309-14

## 7T MRI of the ex vivo perfused rat heart

Lisa Drange-Hole<sup>1,2</sup> Tina Pavlin PhD<sup>2</sup> Terje H. Larsen MD, PhD<sup>2,3</sup> Jan D. Schjøtt MD, PhD<sup>4,5</sup>

<sup>1</sup>School of medicine, University of Bergen, N-5009 Bergen, Norway

<sup>2</sup>Institute of Biomedicine, University of Bergen, N-5009 Bergen, Norway

<sup>3</sup>Department of Heart Disease, Haukeland University Hospital, N-5021 Bergen, Norway

<sup>4</sup>Section of Clinical Pharmacology, Laboratory of Clinical Biochemistry, Haukeland University Hospital, N-5021 Bergen, Norway

<sup>5</sup>Section for Pharmacology, Institute of Internal Medicine, University of Bergen, N-5009 Bergen, Norway

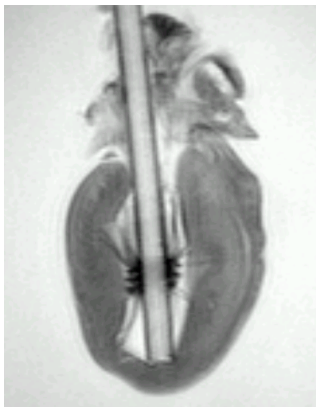
The isolated buffer perfused rat heart represents a high-throughput model for cardiac studies. By manipulation of the composition of perfusate and perfusion mode several pathophysiological conditions can be reproduced in a controlled manner. Furthermore, injection of drugs and contrast agents allows for pharmacological and toxicological experiments. The model eliminates systemic effects associated with heart imaging of intact animals.

**Aim:** To develop a model for imaging of the isolated rat heart in a 7T magnet for very high resolution imaging, including imaging of perfusion variations, viability, coronary vessel morphology, flow and myocardial microstructure.

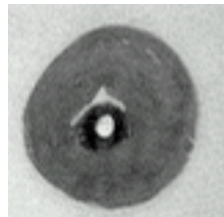
**Method:** An isolated heart system consisting of a water-jacked cylindrical probe with an outer diameter of 40mm was designed. The proximal part of the probe is 100mm, and contains the cannulated and perfused heart in isocenter when the probe is inserted into a horizontal 7T Bruker Pharmascan magnet operating at 300MHz. The magnet has a bore diameter of 160mm and a 1-channel transmit/receive radio frequency volume coil. The isolated rat heart is perfused retrogradely by way of a peristaltic pump. The perfusion supply and drainage lines are embedded together with the heated lines supplying the probe with thermostated water. A side arm for injections is located just outside the magnet. The perfusate is a modified, oxygenated bicarbonate buffer. A water-filled latex balloon is placed in the left ventricle and connected to a pressure transducer for the recording of left ventricular pressure (LVDP), heart rate and secondarily derived contractility indices. The LVDP signal is coupled in parallel with a voltage-sampling unit which triggers image acquisition. A second pressure transducer is connected to a side arm on the aortic cannula just outside the magnet for recording of aortic pressure, as an index of coronary vascular resistance during constant flow perfusion. Physiological parameters are displayed in real time.

**Results:** The isolated heart system adapted for imaging in a horizontal 7T magnet, is now an established method for high field very high resolution imaging to be applied in experimental cardiology.

**Conclusion:** The MRI model offers simultaneously information regarding contractile function, myocardial perfusion, and tissue characteristics regarding oedema and delayed gadolinium enhancement. Thus, it is suitable for the study of various scientific problems in experimental cardiology.



**TurboRARE**  
TR 1200 ms  
TE 36 ms  
FA 180°  
Voxel 0.15 x 0.15 mm  
S Th 2 mm



**FLASH**  
TR 250 ms  
TE 3.7 ms  
FA 75°  
Voxel 0.15 x 0.15 mm  
S Th 2 mm

Wednesday

# **Strategies to Increase the Sensitivity in NMR Spectroscopy**

Dick Sandström

*Bruker BioSpin Scandinavia AB, Vallgatan 5, SE-170 67 Solna, Sweden*

NMR, although extremely useful, is an inherently insensitive spectroscopic method. The aim of this presentation is to introduce recent developments from Bruker BioSpin that push the limits of NMR sensitivity. Topics will include hyperpolarization techniques such as para-hydrogen induced polarization (PHIP) liquid-state NMR and dynamic nuclear polarization (DNP) enhanced solid-state NMR. Recently introduced CryoProbeheads will also be discussed.

## **Amphiphilic drug interaction with glycerophospholipid studied by Solid-State NMR and the Langmuir monolayer technique.**

Signe Steinkopf<sup>1</sup>, Anja Gjerde<sup>2</sup>, Holm Holmsen<sup>2</sup> and Willy Nerdal<sup>3</sup>.

<sup>1</sup>*Department of Biomedical Laboratory Science, Bergen University College,*

<sup>2</sup>*Department of Biomedicine, University of Bergen.*

<sup>3</sup>*Department of Chemistry, University of Bergen.*

Chlorpromazine (CPZ) and olanzapine (OLP) are antipsychotic drugs with an effect ascribed to the antagonism of dopaminergic receptors. However, CPZ interferes with polyphosphoinositide metabolism in simulated platelets. These cells do not contain D<sub>2</sub>-receptors, and CPZ interferes with the platelet membrane structure.

The interactions of CPZ and OLP with glycerophospholipid monolayers show that both increase the mean molecular area (mma) of negatively charged serine head-groups, and that OLP has a larger effect than CPZ. The results are in agreement with findings from a Solid-State NMR study on glycerophospholipid bilayers. Both CPZ and OLP decreased the intensity of the *sn*-3 carbon resonance where the phosphorus and head group are attached. Decreased signal intensity occurred for the serine carboxyl resonance. Further, we have studied the intercalation of OLP in phospholipids of serine, choline, ethanolamine and cholesterolhead-group. OLP increases the mma of all lipids with the exception of cholesterol containing monolayers. Segregation in the DPPS(80%)/DPPE(20%) monolayer occurs, and OLP interaction demonstrates that the monolayer segregation of lipids disappears. Results from Solid-State NMR show the presence of microdomains in the DPPC/SDPC bilayer. When CPZ is added, the microdomains disappears. CPZ might affect the area occupied by a SDPS molecule in the bilayer. It is likely that such CPZ and OLP induced changes can affect the function of proteins embedded in the bilayer.

## Chain Diffusion in Semi-Crystalline Polymers (Modelling of the carbon Spin-Lattice Relaxation Curve)

Eddy Walther Hansen  
Department of Chemistry/UiO  
e-mail: eddywh@kjemi.uio.no

**Abstract:** A semi-crystalline polymer may be considered as crystallites embedded in an amorphous matrix in which the former are made up of chains forming ordered, lamellar structures (Figure 1). In contrast, the amorphous phase (matrix) is composed of randomly distributed chains possessing no long-range order. In general, a polymer chain may typically extend over several lamellae and thus be part of both the crystalline- and the amorphous regions.

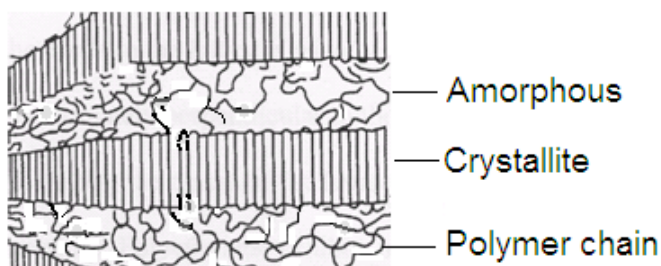


**Figure 1.** Crystalline and amorphous domains of a semi-crystalline polymer

It is well known that polymer chains possess significant molecular motion, even at room temperature. For instance, polymer chains may exchange between crystalline- and amorphous domains (and visa versa) by a diffusion process. Since these motions affect the macroscopic properties of the polymer it is of importance to probe these dynamic features.

Based on the classical Fick-diffusion concept, a model is presented which enables the chain diffusivity to be determined from carbon spin-lattice relaxation data.

## **Dynamic NMR: Pore structure characterization and pore scale connectivity**

Ketil Djurhuus

Accurate estimates of fluid flow functions are of vital importance to the successful extraction of hydrocarbons. Absolute permeability is one of the most important parameters describing fluid flow, but can be difficult to measure outside the laboratory. It is therefore of great interest to relate other more easily measured properties of porous rocks to the permeability.

In restricted geometries such as saturated porous media, the apparent diffusion coefficient of a confined fluid depends on observation time. From the time dependency of the diffusion coefficient, information about the geometrical properties of the porous medium can be obtained. Pulsed field gradient NMR constitute an excellent means of measuring diffusion coefficient time dependency. From the shortest diffusion times, the surface-to-volume ratio can be extracted to resolve the surface relaxivity in regular relaxation time distributions, whereas the long time behavior of the diffusion coefficient proves to hold information about the micro connectivity of the pore network.

## Water and Heptanol Interaction with a Non-porous Silica Surface: A $^1\text{H}$ Solid State NMR Study

*Christian Totland, Signe Steinkopf, Anne Marit Blokhus, Willy Nerdal*

### Abstract:

Colloidal, non-porous and uniform silica particles with a diameter of 40 nm were used in this study as a model rock carrying water and hydrocarbon. The samples were prepared so that the amount of bulk liquid was reduced to a minimum, making the study of surface interactions possible using conventional NMR methods.

Static  $^1\text{H}$ -NMR spectra displays broad water/hydrocarbon resonances. The resonances of the various water samples show specific line shapes that are consistent over several similar samples.

Detailed information about the interaction at the silica surface is obtained by  $^1\text{H}$ -MAS NMR where the spin-lattice ( $T_1$ ) relaxation behaviour of water and heptanol is monitored as a function of temperature.

Reorientation activation energies,  $E_a$ , are extracted from the temperature dependence of the molecular correlation times,  $\tau_c$ . The temperature dependence of each chemically equivalent proton group in the molecule could be assessed due to the resolved  $^1\text{H}$ -MAS spectra.

The values of  $E_a$  indicate a varying degree of rotational freedom within the heptanol molecule, due to the interaction of the hydroxyl group with the silica surface.  $E_a$  values of water also demonstrate a decrease in rotational freedom of surface bound water molecules. However, when a small amount of heptanol is introduced into the water/silica system, the rotational freedom of water increases.

# Cisplatin interaction with phosphatidylserine bilayer studied by solid-state NMR spectroscopy

Willy Nerdal<sup>1</sup>, Morten Bjerring<sup>2</sup>, Niels Christian Nielsen<sup>2</sup> and Magnus Jensen<sup>1</sup>

<sup>1</sup>Department of Chemistry, University of Bergen, Allegaten 41, N5007 Bergen, Norway.

<sup>2</sup>Department of Chemistry, University of Aarhus, Langelandsgade 140, DK-8000 Aarhus C, Denmark.

Cisplatin (*cis*-Diamminedichloridoplatinum(II)) is used in chemotherapy and it is well established that cisplatin forms platinum-DNA adducts that initiate tumor cell death.

Drawbacks are side effects such as neurotoxicity and cellular cisplatin resistance and it is possible that some of these effects are linked to cisplatin interaction with lipids and the phospholipid bilayer. <sup>13</sup>C magic angle spinning (MAS) nuclear magnetic resonance (NMR) spectra of bilayer formed by total lipid extract from pig brain with and without cisplatin show cisplatin binding to the serine head group in phosphatidylserine and static and MAS <sup>31</sup>P NMR spectra demonstrate cisplatin induced isotropic and/or hexagonal lipid phases (1). Cisplatin interaction with phosphatidylserine bilayer has been studied by <sup>15</sup>N{<sup>31</sup>P} rotational-echo double resonance NMR (2) providing interatomic distances of a cisplatin-phosphatidylserine complex. The data show deamination of cisplatin when bound to the serine head group.

†This work was supported by the Norwegian Research Council (NFR).

1. Jensen, M., Nerdal, W., 2008. Anticancer cisplatin interactions with bilayers of total lipid extract from pig brain: A <sup>13</sup>C, <sup>31</sup>P and <sup>15</sup>N solid-state NMR study. *Eur. J. Pharm. Sci.*, 34, 140 – 148.

2. Gullion, T., Shaefer, J., 1989. Rotational-Echo Double-Resonance NMR. *J. Magn. Reson.* 81, 196 – 200.

# Posters

## Segmental labelled AlgE4 - an alginate epimerase

Buchinger, Edith<sup>1</sup>; Aachmann, Finn L<sup>2</sup>.; Skjåk-Bræk, Gudmund<sup>2</sup>; Valla, Svein<sup>2</sup>; Iwai, Hideo<sup>3</sup>; Wimmer, Reinhard<sup>1</sup>.

<sup>1</sup>Aalborg University, Department of Biotechnology, Chemistry and Environ, Aalborg, Denmark; <sup>2</sup>Norwegian University of Science and Technology, NOBIPOL, Department of Biotechnology, Trondheim, Norway; <sup>3</sup>University of Helsinki, Institute of Biotechnology, Helsinki, Finland.

Nuclear magnetic resonance (NMR) is a powerful method to determine protein dynamics and protein-ligand interactions. New NMR techniques have extended the size limit for the observation of NMR signals to over 100kDa, but signal overlap in large proteins can hinder spectral analysis. Isotopic labelling of only a segment of a large protein reduces the spectral complexity but still allows sequence-specific resonance assignment and functional investigations.

One method of segmental isotopic labelling relies on the protein splicing activity of split inteins. Protein splicing needs no cofactors or reagents to excise an intervening sequence and ligate two flanking N- and C-terminal segments via a peptide bond. Additionally, the ligation of segments can be done *in vivo* or *in vitro*.

In the bacterium *Azotobacter vinelandii*, a family of seven secreted and calcium-dependent mannuronan C-5 epimerases (AlgE1–7) has been identified. These epimerases are responsible for the epimerization of  $\beta$ -D-mannuronic (M) acid to  $\alpha$ -L-guluronic acid (G) in alginate polymers. The epimerases consist of two types of structural modules, designated A [ $\sim$ 350aa] (one or two copies) and R [ $\sim$ 150aa] (one to seven copies). Each member of the AlgE-family produces a unique sequence of M and G subunits. The A-modules are catalytic active; the R-modules strongly enhance this activity although they don't possess any catalytic activity. The smallest member of the family, AlgE4, consists of one A- and one R-module (A-R). The structure of the A-module of AlgE4 has been solved by X-ray crystallography and the structure of the R-module was solved by NMR spectroscopy. NMR studies on the R-module of AlgE4 have shown that alginate also binds to the R-module. The function of the R-domains in the AlgE-family is to a large extent unknown.

Our objective is to obtain an active segmentally labelled AlgE4 (14N-A-15N-R) for alginate binding studies to the R-module by NMR. For the protein splicing we used the naturally split intein of *Nostoc punctiformae*. Finally, a multiple segmentally labelled AlgE4 will be produced for interaction studies between both modules with and without alginate.

## Field dependence of longitudinal relaxation contrast in cardiac manganese enhanced MRI

John Georg Seland<sup>1</sup>, Morten Bruvold<sup>2</sup>, Tina Pavlin<sup>2</sup>, Per Jynge<sup>3</sup>

<sup>1</sup>Department of Chemistry, University of Bergen, Bergen, Norway, <sup>2</sup>Department of Circulation and Medical Imaging, Norwegian University of Science and Technology, Trondheim, Norway, <sup>3</sup>Department of Pharmacology, Linköping University, Linköping, Sweden.

**Background.** Manganese ions ( $Mn^{2+}$ ) are able to enter excitable cells, where they bind to intracellular sites, resulting in a significant increase in the longitudinal relaxation rate ( $R_1=1/T_1$ ). To investigate the underlying relaxation mechanism, we measured the *in vivo* longitudinal relaxation rate enhancement ( $\Delta R_1$ ) in  $Mn^{2+}$ -enriched rat heart tissue (left ventricle myocardium) at two different magnetic field strengths (2.35 and 7.0 T), and compared the experimental data to theoretical simulations using the Solomon-Bloembergen-Morgan (SBM) equations.

**Results and Discussion.** When adding a dose of  $60 \mu\text{mol/kg } Mn^{2+}$ , the experimental data showed that  $\Delta R_1$  was  $0.85$  and  $0.55 \text{ s}^{-1}$ , at respectively 2.35 and 7.0 T. In our simulations we assumed that  $Mn^{2+}$  forms an intracellular macromolecular complex, which can be treated as a conventional metal chelate. It is then the so-called inner-sphere relaxivity,  $r_1$  that determines the relaxation properties of the molecule. The relative change in  $r_1$  and  $\Delta R_1$  will be the same when changing the magnetic field strength. Using the SBM equations we therefore calculated  $r_1$  at different magnetic field strengths, and compared it to the change in  $\Delta R_1$ . In particular we focused on the rotational correlation time,  $\tau_R$ , and the water exchange time,  $\tau_m$ , which are the two most important parameters influencing  $r_1$ . For details regarding the SBM equations, we refer to the review paper by Lauffer [1], and to Aime *et al.* [2] for manganese complexes in particular.

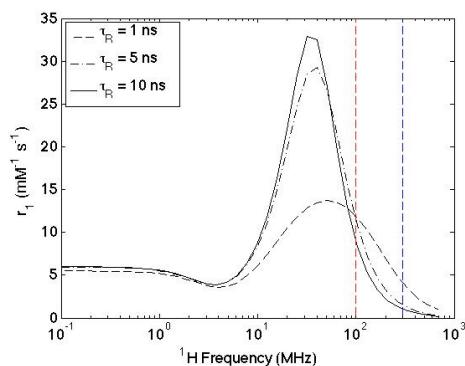


**Figure 1.** Simulation of inner-sphere relaxivity,  $r_1$ , as a function of magnetic field strength, and at three different values of the rotational correlation time,  $\tau_R$  (other parameter values [2]:  $S=5/2$ ,  $r=3.1\text{\AA}$ ,  $q=1$ ,  $\tau_m=5\text{ns}$ ,  $\tau_v=30\text{ps}$  and  $\Delta T^2=5 \cdot 10^{19} \text{ s}^{-2}$ ). The relative decrease in  $r_1$  from 2.35 to 7.0 T (corresponding to respectively 100 and 300 MHz, as indicated by the vertical lines) is larger at longer  $\tau_R$ . The decrease in  $\Delta R_1$  of 35% observed in our experiments is best described by the curve for  $\tau_R = 1 \text{ ns}$ , but leads to absolute values of  $r_1$  significantly lower than observed experimentally [3]. For longer  $\tau_R$  correct absolute values of  $r_1$  is obtained, but the field dependent decrease is then too large. The results therefore indicates that  $Mn^{2+}$  binds to various intracellular sites, leading to a rather broad distribution of  $\tau_R$  values, with a corresponding distribution of responses on  $r_1$  with respect to the magnetic field strength.

(A)

(B)

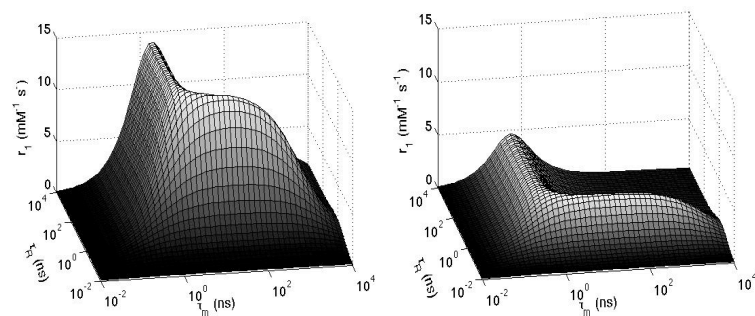


**Figure 2.** Simulation of the interplay between  $\tau_R$  and  $\tau_m$  on the inner-sphere relaxivity,  $r_1$  ( $q = 1$  and  $r = 3.1\text{\AA}$  and  $T_{1e} = 10 \text{ ns}$ ) at 2.35T (A) and 7.0T (B). Expected values for  $\tau_R$  and  $\tau_m$  in a larger  $Mn^{2+}$  complex is approximately 1 and 5 ns, respectively [4], corresponding to a peak in the relaxivity. In comparison,  $\tau_R$  in a small extracellular metal complex is much less than 1 ns [1], leading to a lower relaxivity compared to an intracellular  $Mn^{2+}$  complex. The sharp and intense edge in (B) at  $\tau_R=1\text{ns}$  indicates that it is more favorable to perform cardiac manganese enhanced MRI at low fields.

**Conclusion.** Our experimental results together with theoretical simulations indicate that  $Mn^{2+}$  binds to a broad range of intracellular sites, leading to a distribution of rotational correlation times  $\tau_R$  and increased relaxivities  $r_1$ . This range of  $\tau_R$  values also indicate that it is favorable to perform cardiac manganese enhanced MRI at relatively low magnetic fields.

### References.

- [1] RB. Lauffer, *Chemical Reviews*, **87** (5), 901-927, (1987). [2] S. Aime *et al.* *J Biol Inorg Chem*, **7** (1-2), 58-67, (2007). [3] JG. Seland, *et al.* *Magn. Reson. Med.* **58**, 674-686, (2007). [4] SC. Jackels, *et al.* *Inorganic Chemistry*, **31**, 234-239, (1992).

Abstract poster to National NMR Meeting (NMR 2010):

Sara Marie Øie Solbak, Karsten Bruns, Nicole Studtrucker, Alok Sharma, Rene Röder, David Mitzner, Friedrich Hahn, André Eissmann, Uwe Tessmer, Peter Henklein, Torgils Fossen, Victor Wray, Ulrich Schubert

## **Structural characterization of PB1-F2 influenza A virus proteins**

The proapoptotic influenza A (IAV) virus PB1-F2 protein contributes to viral pathogenicity and is present in most human and avian isolates. The full length structure of PB1-F2 encoded by the H1N1 human isolates A/Puerto Rico/8/34 and 'Spanish flu' H1N1 A/Brevig Mission/1/1918 have been characterised by NMR spectroscopy. <sup>1</sup>H NMR analysis of three overlapping peptides and the full-length protein afforded direct experimental evidence of the presence of a C-terminal region with strong  $\alpha$ -helical propensity comprising amino acid residues.

### **References**

K. Bruns, N. Studtrucker, A. Sharma, T. Fossen, D. Mitzner, A. Eissmann, U. Tessmer, R. Roder, P. Henklein, V. Wray, U. Schubert: Structural characterization and Oligomerization of PB1-F2, a pro - apoptotic influenza A virus protein. *Journal of Biological Chemistry*, 2007, 282, 353-363.

R. Röder, K. Bruns, A. Sharma, A. Eissmann, F. Hahn, N. Studtrucker, T. Fossen, V. Wray, P. Henklein, U. Schubert (2008). Synthesis of full length PB1-F2 influenza A virus proteins from 'Spanish flu' and 'bird flu'. *Journal of Peptide Science* 14, 954-962.